

# $^{10}\text{B}+\alpha$ states with chain-like structures in $^{14}\text{N}$

Yoshiko Kanada-En'yo

Department of Physics, Kyoto University, Kyoto 606-8502, Japan

I investigate  $^{10}\text{B}+\alpha$  cluster states of  $^{14}\text{N}$  with a  $^{10}\text{B}+\alpha$  cluster model. Near the  $\alpha$ -decay threshold energy, I obtain  $K^\pi = 3^+$  and  $K^\pi = 1^+$  rotational bands having  $^{10}\text{B}(3^+)+\alpha$  and  $^{10}\text{B}(1^+)+\alpha$  components, respectively. I assign the band-head state of the  $K^\pi = 3^+$  band to the experimental  $3^+$  at  $E_x=13.19$  MeV of  $^{14}\text{N}$  observed in  $\alpha$  scattering reactions by  $^{10}\text{B}$  and show that the calculated  $\alpha$ -decay width is consistent with the experimental data. I discuss an  $\alpha$ -cluster motion around the  $^{10}\text{B}$  cluster and show that  $^{10}\text{B}+\alpha$  cluster states contain significant components of a linear-chain  $3\alpha$  configuration, in which an  $\alpha$  cluster is localized in the longitudinal direction around the deformed  $^{10}\text{B}$  cluster.

## I. INTRODUCTION

It is known that cluster structures appear in various nuclei including unstable nuclei (for instance, [1–5] and references therein.) For cluster states having an  $\alpha$  cluster around a core nucleus, well-known examples are  $^{16}\text{O}+\alpha$  states in  $^{20}\text{Ne}$  and  $^{12}\text{C}+\alpha$  states in  $^{16}\text{O}$  [6]. Recent experimental and theoretical studies have revealed many cluster resonances in highly excited states near the  $\alpha$ -decay threshold also in unstable nuclei, for instance,  $A-4\text{He}+\alpha$  states in Be isotopes [1, 4, 7–26],  $^{10}\text{Be}+\alpha$  states in  $^{14}\text{C}$  [27–30, 54],  $^{14}\text{C}+\alpha$  states in  $^{18}\text{O}$  and their mirror states [31–40],  $^{18}\text{O}+\alpha$  states in  $^{22}\text{Ne}$  [38–45].

Multi- $\alpha$  cluster states such as cluster gas and linear-chain states of  $n\alpha$  systems are also interesting topics. The  $\alpha$ -cluster gas was proposed by Tohsaki *et al.* to describe  $3\alpha$  cluster structure of  $^{12}\text{C}(0_2^+)$  [46] and extended to excited states of  $^{12}\text{C}$  and other nuclei [47–49]. The linear-chain  $n\alpha$  state was originally proposed for  $^{12}\text{C}(0_2^+)$  by Morinaga in the 1950-60s [50, 51]. However, in the 1970s, this picture was excluded at least for  $^{12}\text{C}(0_2^+)$  having a larger  $\alpha$ -decay width than the one expected from the linear-chain structure [52]. In spite of many discussions for several decades, existence of linear-chain  $n\alpha$  states have yet been confirmed and it is still an open problem to be solved. It is naively expected that the linear-chain configuration is not favored in an  $n\alpha$  system because it costs much kinetic energy to keep  $\alpha$  clusters in a row. It means that some mechanism is necessary to form the linear-chain structure. In progress of physics of unstable nuclei since the 1990s, it was proposed for neutron-rich C isotopes that excess neutrons may stabilize the linear-chain structure [1, 8]. Itagaki *et al.* analyzed stability of a  $3\alpha$ -chain configuration surrounded by excess neutrons in molecular orbitals against the bending motion and suggested that the linear-chain structure can be stable in  $^{16}\text{C}$  but unstable in  $^{12}\text{C}$  and  $^{14}\text{C}$  [53]. More recently, Suhara and the author predicted a rotational band with a linear  $3\alpha$  chain configuration in excited states of  $^{14}\text{C}$  near the  $\alpha$ -decay threshold [54]. They pointed out that the orthogonal condition to lower states is important for the stability of the linear-chain structure. The linear-chain structure is expected to be more favored in high spin states because of stretching effect in rotating systems as suggested in  $^{15}\text{C}$  [1] and  $^{16}\text{O}$  [55].

According to analysis in Refs. [54, 56], linear-chain states of  $^{14}\text{C}$  are found to have a  $2\alpha + 2n$  correlation and are interpreted as  $^{10}\text{Be}+\alpha$  structures, where the  $^{10}\text{Be}$  cluster is a prolately deformed state containing a  $2\alpha$  core and an additional  $\alpha$  cluster is located in the longitudinal direction of the  $^{10}\text{B}$  cluster. Similarly, the linear-chain state of  $^{15}\text{C}$  suggested in Ref. [1] also shows a  $^{11}\text{Be}+\alpha$  cluster structure with a prolately deformed  $^{11}\text{Be}$  cluster and an  $\alpha$  cluster in the longitudinal direction. It means that, the linear-chain states in these neutron-rich C tend to have the  $2\alpha$  correlation, and therefore  $3\alpha$  linear-chain structures are expected to be found in  $\text{Be}+\alpha$  cluster states.

In this paper, I focus on  $^{10}\text{B}+\alpha$  cluster states in excited states of  $^{14}\text{N}$ . In experimental energy levels of  $^{14}\text{N}$  near the  $\alpha$ -decay threshold,  $J^\pi = 3^+$  and  $1^+$  resonances were observed by  $\alpha$  elastic scattering by  $^{10}\text{B}$  [57]. These resonances are expected to be  $^{10}\text{B}+\alpha$  cluster states because of significant  $\alpha$ -decay widths. In analogy to  $^{10}\text{Be}+\alpha$  cluster states, it is interesting to investigate whether  $^{10}\text{B}+\alpha$  cluster states with the dominant linear-chain structure exist. The ground state ( $3^+$ ) and the first excited state ( $1^+$ ) of  $^{10}\text{B}$  can be described by the deformed state with a  $2\alpha$  core surrounded by  $pn$  as discussed in Refs. [7, 58]. If a  $^{10}\text{B}+\alpha$  cluster state has an  $\alpha$  cluster in the longitudinal direction of the deformed  $^{10}\text{B}$  cluster, the  $^{10}\text{B}+\alpha$  cluster state can be interpreted as a kind of linear-chain state that contains dominantly  $3\alpha$  clusters arranged in a row.

My aim is to study  $^{10}\text{B}+\alpha$  cluster states of  $^{14}\text{N}$  and discuss  $3\alpha$  configurations, in particular, the linear-chain component in  $^{10}\text{B}+\alpha$  cluster states. I calculate  $^{10}\text{B}(3^+) \otimes L_\alpha$  and  $^{10}\text{B}(1^+) \otimes L_\alpha$  components and evaluate partial  $\alpha$ -decay widths of  $^{10}\text{B}+\alpha$  cluster states. To discuss stability of the linear-chain  $^{10}\text{B}+\alpha$  structure, I analyze angular motion of an  $\alpha$  cluster around the deformed  $^{10}\text{B}$  cluster, i.e., rotation of the  $^{10}\text{B}$  cluster.

This paper is organized as follows. In Sec. II, I explain the formulation of the present  $^{10}\text{B}+\alpha$  cluster model. In Sec. III, calculated positive-parity states and  $E2$  transition strengths of  $^{14}\text{N}$  are shown. I discuss  $\alpha$  cluster motion

around  $^{10}\text{B}(3^+)$  and  $^{10}\text{B}(1^+)$  in Sec. IV. Finally, a summary is given in Sec. V.

## II. FORMULATION OF THE $^{10}\text{B}+\alpha$ CLUSTER MODEL

### A. Description of the $^{10}\text{B}$ cluster

For the  $^{10}\text{B}$  cluster in the present  $^{10}\text{B}+\alpha$  cluster model, I adopt a  $2\alpha + (pn)$  wave function which can reasonably describe features of the ground ( $J^\pi = 3^+$ ) and first excited ( $1^+$ ) states of  $^{10}\text{B}$  as discussed in Ref. [58]. The  $2\alpha + (pn)$  wave function is given by a three-body cluster wave function, where  $\alpha$  clusters and a dinucleon ( $pn$ ) cluster are written by  $(0s)^4$  and  $(0s)^2$  harmonic oscillator configurations, respectively, as

$$\Phi_{2\alpha+pn}(\mathbf{R}_1, \mathbf{R}_2, \mathbf{R}_3) = \mathcal{A}\{\Phi_\alpha(\mathbf{R}_1)\Phi_\alpha(\mathbf{R}_2)\Phi_{pn}(\mathbf{R}_3)\}, \quad (1)$$

$$\Phi_\alpha(\mathbf{R}) = \psi_{p\uparrow}(\mathbf{R})\psi_{p\downarrow}(\mathbf{R})\psi_{n\uparrow}(\mathbf{R})\psi_{n\downarrow}(\mathbf{R}), \quad (2)$$

$$\Phi_{pn}(\mathbf{R}) = \psi_{p\uparrow}(\mathbf{R})\psi_{n\uparrow}(\mathbf{R}), \quad (3)$$

$$\psi_\sigma(\mathbf{R}) = \varphi_{0s}(\mathbf{R})\chi_\sigma, \quad (4)$$

where  $\mathcal{A}$  is the antisymmetrizer for all nucleons and  $\varphi_{0s}(\mathbf{R})$  is the spatial part of the single-particle wave function of the  $0s$  orbit around  $\mathbf{R}$ ;

$$\varphi_{0s}(\mathbf{R}) = \left(\frac{2\nu}{\pi}\right)^{3/4} \exp\{-\nu(\mathbf{r} - \mathbf{R})^2\}, \quad (5)$$

and  $\chi_\sigma$  is the spin-isospin wave function for  $\sigma = p\uparrow, p\downarrow, n\uparrow,$  and  $n\downarrow$ . For the  $^{10}\text{B}$  cluster, I set 2  $\alpha$  clusters in the  $z$  direction as  $\mathbf{R}_1 - \mathbf{R}_2 = (0, 0, d_{2\alpha})$  with  $d_{2\alpha} = 3$  fm and a spin-aligned  $pn$  cluster on the  $x$ - $y$  plane at the distance  $d$  from the  $2\alpha$  center as  $\mathbf{R}_3 - (\mathbf{R}_1 + \mathbf{R}_2)/2 = (d\cos\phi, d\sin\phi, 0)$ . I write the  $^{10}\text{B}$  wave function localized around  $\mathbf{X}_B \equiv (4\mathbf{R}_1 + 4\mathbf{R}_2 + 2\mathbf{R}_3)/10$  as  $\Phi_{^{10}\text{B}}(\mathbf{X}_B; d, \phi)$  with the center position  $\mathbf{X}_B$  and the distance and angle parameters,  $d$  and  $\phi$ , for the  $pn$  cluster position. In the  $^{10}\text{B}+\alpha$  cluster model, I superpose the  $^{10}\text{B}$  wave functions with  $d = 1, 2$  (fm) and  $\phi_j = \frac{\pi}{4}(j - 0.5)$  ( $j = 1, \dots, 8$ ). Parity ( $\pi$ ) and  $K$  ( $I_z$ ) projections of the subsystem  $^{10}\text{B}$  can be approximately done by the  $\phi_j$  summation;

$$\Phi_{^{10}\text{B}(I_z^\pi)}(\mathbf{X}_B; d) = \sum_j c_j \Phi_{^{10}\text{B}}(\mathbf{X}_B; d, \phi_j) \quad (6)$$

with  $c_j = \exp(i(I_z - 1)\phi_j)$  and  $\pi = (-1)^{I_z - 1}$ . Here,  $I_z$  is the  $z$  component of the total angular momentum  $\mathbf{I}$  of  $^{10}\text{B}$  and is given by a sum of the aligned intrinsic spin  $S_z = 1$  and the orbital  $\phi$  rotation of the  $pn$  cluster. It is clear that  $\phi_j$  superposition with given coefficients  $c_j$  is equivalent to  $I_z$  mixing.

### B. $^{14}\text{N}$ wave function in the $^{10}\text{B} + \alpha$ model

A  $^{10}\text{B} + \alpha$  wave function is written using the  $^{10}\text{B}$  wave function  $\Phi_{^{10}\text{B}}(\mathbf{X}_B; d, \phi)$  and the  $\alpha$ -cluster wave function  $\Phi_\alpha(\mathbf{X}_\alpha)$  as

$$\Phi_{^{10}\text{B}+\alpha}(D_\alpha, \theta_\alpha; d, \phi) = \mathcal{A}\{\Phi_{^{10}\text{B}}(\mathbf{X}_B; d, \phi)\Phi_\alpha(\mathbf{X}_\alpha)\}, \quad (7)$$

where  $\mathbf{X}_\alpha - \mathbf{X}_B = (D_\alpha \sin\theta_\alpha, 0, D_\alpha \cos\theta_\alpha)$ . Here the distance  $D_\alpha$  and the angle  $\theta_\alpha$  indicate the  $\alpha$ -cluster position relative to the deformed  $^{10}\text{B}$  cluster (see Fig. 1). The center of mass position is taken to be  $4\mathbf{X}_\alpha + 10\mathbf{X}_B = 0$  so as to decouple the center of mass motion and the intrinsic wave function. Wave functions for the  $J_n^\pi$  states of  $^{14}\text{N}$  are expressed by superposition of the  $J^\pi$ -projected wave functions as

$$\Psi_{^{14}\text{N}(J_n^\pi)} = \sum_K \sum_{D_\alpha, \theta_\alpha} \sum_{d, \phi} C(K, D_\alpha, \theta_\alpha, d, \phi) \hat{P}_{MK}^{J_n^\pi} \Phi_{^{10}\text{B}+\alpha}(D_\alpha, \theta_\alpha; d, \phi), \quad (8)$$

where  $\hat{P}_{MK}^{J_n^\pi}$  is the parity and total angular momentum projection operator. Coefficients  $C(K, D_\alpha, \theta_\alpha, d, \phi)$  are determined by diagonalizing Hamiltonian and norm matrices. I take  $D_\alpha = \{2, \dots, 6\}$  (fm),  $\theta_\alpha = \{0, \pi/4, \pi/2\}$ ,  $d = \{1, 2\}$  (fm), and  $\phi = \frac{\pi}{4}(j - 0.5)$  ( $j = 1, \dots, 8$ ). In the present paper, I calculate positive-parity ( $\pi = +$ ) states of  $^{14}\text{N}$ .

In Eq. (8), coupling of  $\mathbf{I}$  (the spin of the  $^{10}\text{B}$  cluster) and  $\mathbf{L}_\alpha$  (the orbital angular momentum of the  $\alpha$  cluster relative to the  $^{10}\text{B}$  cluster) is implicitly described by the  $J^\pi$  projection,  $K$  mixing, and  $\theta_\alpha, \phi$  summations. As shown in Fig. 1,  $\mathbf{L}_\alpha$  couples with  $\mathbf{I}$  to the total angular momentum  $\mathbf{J} = \mathbf{L}_\alpha + \mathbf{I}$ . The  $z$  component,  $J_z = I_z + L_{\alpha z}$ , is the so-called  $K$  quantum. Strictly speaking,  $L_\alpha = 0, 2$  ( $S, D$ -wave) mixing is approximately taken into account by the summation of  $\theta_\alpha = \{0, \pi/4, \pi/2\}$  but higher  $L_\alpha (\geq 4)$  mixing can not be controlled in the present calculation because of the finite number of mesh points for  $\theta_\alpha$ .

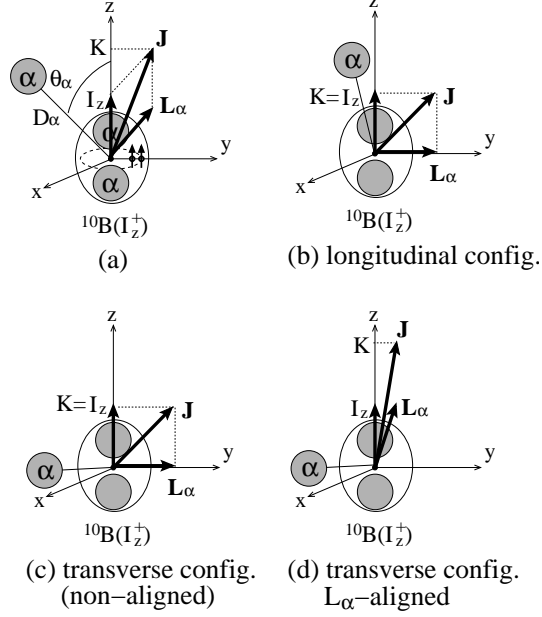


FIG. 1: Schematic figures for  $^{10}\text{B}+\alpha$  configurations. (a) Parameters of the  $^{10}\text{B}+\alpha$  cluster model. (b) Longitudinal configuration for  $\theta_\alpha \sim 0$ , (c) transverse configuration for  $\theta_\alpha \sim \pi/2$  without  $L_\alpha$  alignment, and (d)  $L_\alpha$ -aligned transverse configuration.

### C. Overlap function and $\alpha$ -cluster probability

In order to evaluate  $^{10}\text{B}(3^+) \otimes L_\alpha$  and  $^{10}\text{B}(1^+) \otimes L_\alpha$  components at a channel radius ( $D_\alpha$ ), I consider the  $L_\alpha L_{\alpha z}$  projected  $^{10}\text{B}(I_z^\pi) + \alpha$  wave function,

$$|J^\pi K; ^{10}\text{B}(I_z^\pi); D_\alpha, L_\alpha L_{\alpha z}\rangle = n_0 \sum_{\theta_\alpha} \omega(\theta_\alpha) Y_{L_\alpha}^{L_\alpha}(\theta_\alpha) \hat{P}_{MK}^{J^\pi} \Phi_{^{10}\text{B}(I_z^\pi)+\alpha}(D_\alpha, \theta_\alpha), \quad (9)$$

$$\Phi_{^{10}\text{B}(I_z^\pi)+\alpha}(D_\alpha, \theta_\alpha) = \mathcal{A} \{ \Phi_{^{10}\text{B}(I_z^\pi)}(\mathbf{X}_B; d) \Phi_\alpha(\mathbf{X}_\alpha) \}, \quad (10)$$

with  $I_z = \{1, 3\}$ ,  $\pi = +$ ,  $K = I_z + L_{\alpha z}$ ,  $\mathbf{X}_\alpha - \mathbf{X}_B = (D_\alpha \sin \theta_\alpha, 0, D_\alpha \cos \theta_\alpha)$ , and  $4\mathbf{X}_\alpha + 10\mathbf{X}_B = 0$ .  $Y_\mu^\lambda$  is the spherical harmonics.  $\Phi_{^{10}\text{B}(I_z^\pi)+\alpha}(D_\alpha, \theta_\alpha)$  is the wave function for the  $\alpha$  cluster at  $(D_\alpha, \theta_\alpha)$  around the  $I_z$  projected  $^{10}\text{B}$  cluster, for which I fix  $d = 2$  fm in the present analysis.  $n_0$  is determined from the normalization condition  $\langle JK; ^{10}\text{B}(I_z^\pi); D_\alpha, L_\alpha L_{\alpha z} | JK; ^{10}\text{B}(I_z^\pi); D_\alpha, L_\alpha L_{\alpha z} \rangle = 1$ . In Eq. (9), the  $L_\alpha L_{\alpha z}$  projection is approximately performed by the summation  $\theta_\alpha = \frac{\pi}{N_\theta} i$  ( $i = 0, \dots, N_\theta$ ) with the weight function  $\omega(\theta_\alpha) = \int_{\min[\theta_\alpha - \pi/2N_\theta, 0]}^{\max[\theta_\alpha + \pi/2N_\theta, \pi]} \sin \theta d\theta$ . I perform only  $L_\alpha = 0, 2$  projections because  $L_\alpha \geq 4$  projections are not possible for the present  $N_\theta = 4$  case. I calculate the squared overlap of the  $^{14}\text{N}$  wave function with the above wave function,  $|\langle JK; ^{10}\text{B}(I_z^\pi); D_\alpha, L_\alpha L_{\alpha z} | \Psi_{^{14}\text{N}(J_\pi^\pi)} \rangle|^2$ . Assuming that the  $3_1^+$  and  $1_1^+$  states of the  $^{10}\text{B}$  cluster are approximately described by the  $I_z$  projected  $^{10}\text{B}$  wave functions,  $^{10}\text{B}(I_z^\pi = 3^+)$  and  $^{10}\text{B}(I_z^\pi = 1^+)$ , respectively, I approximately estimate the  $^{10}\text{B}(I^\pi) \otimes (L_\alpha = 0, 2)$  components as

$$P_{^{10}\text{B}(I^\pi) \otimes L_\alpha}(D_\alpha) \approx \sum_{L_\alpha z} |\langle JK | I I_z L_\alpha L_{\alpha z} \rangle \langle JK; ^{10}\text{B}(I_z); D_\alpha, L_\alpha L_{\alpha z} | \Psi_{^{14}\text{N}(J_\pi^\pi)} \rangle|^2 \quad (11)$$

with  $I_z = I$ , where  $\langle JK | I I_z L_\alpha L_{\alpha z} \rangle$  is the Clebsch-Gordan coefficient.

I also calculate  $\alpha$ -cluster probability at  $(D_\alpha, \theta_\alpha)$  around the  $I_z$  projected  $^{10}\text{B}$  cluster as

$$P(JK; ^{10}\text{B}(I_z^\pi); D_\alpha, \theta_\alpha) = |\langle JK; D_\alpha, \theta_\alpha; ^{10}\text{B}(I_z^\pi) | \Psi_{^{14}\text{N}(J_z^\pi)} \rangle|^2, \quad (12)$$

$$|\langle JK; ^{10}\text{B}(I_z^\pi); D_\alpha, \theta_\alpha \rangle = n_0 \hat{P}_{MK}^{J+} \Phi_{^{10}\text{B}(I_z^\pi)+\alpha}(D_\alpha, \theta_\alpha). \quad (13)$$

The probability  $P(JK; ^{10}\text{B}(I_z^\pi); D_\alpha, \theta_\alpha)$  is useful to discuss geometric configurations of  $3\alpha$  clusters in  $^{10}\text{B}+\alpha$  cluster states in the strong coupling picture. For instance,  $P(JK; ^{10}\text{B}(I_z^\pi); D_\alpha, \theta_\alpha)$  for  $\theta_\alpha \sim 0$  means the component of the ‘‘longitudinal’’ configuration, where the  $\alpha$  cluster is localized in the longitudinal direction of the deformed  $^{10}\text{B}(I_z^\pi)$  cluster. This configuration corresponds to the linear-chain structure as 3  $\alpha$  clusters are arranged in a row as shown in Fig. 1(b). Because of the axial symmetry, the longitudinal configuration contains only  $K = I_z$  ( $L_{\alpha z} = 0$ ) component. For  $\theta_\alpha \sim \pi/2$ ,  $P(JK; ^{10}\text{B}(I_z^\pi); D_\alpha, \theta_\alpha)$  indicates the component of the ‘‘transverse configuration’’ for the  $\alpha$  cluster in the transverse direction of the deformed  $^{10}\text{B}(I_z^\pi)$  cluster. The transverse configuration contains  $K \neq I_z$  components corresponding to the alignment of  $\mathbf{L}_\alpha$  to the spin of the  $pn$ -cluster ( $I_z$ ) in the  $^{10}\text{B}$  cluster as well as the  $K = I_z$  component (see Fig. 1(b) and (c)).

### III. RESULTS

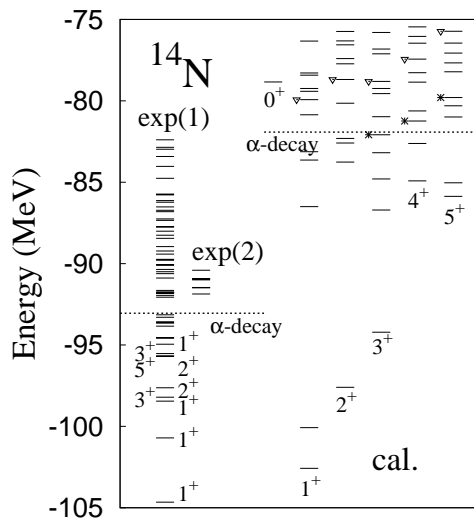


FIG. 2: Positive-parity energy levels of  $^{14}\text{N}$  obtained by the  $^{10}\text{B}+\alpha$  cluster model compared with experimental levels taken from [61].  $^{10}\text{B}+\alpha$  cluster states in the  $K^\pi = 3^+$  band and those in the  $K^\pi = 1^+$  band are labeled by asterisk and down-triangle symbols, respectively.

I adopt the two-body effective nuclear interactions used in Ref. [58] which are adjusted to describe low-lying energy levels of  $^{10}\text{B}$ . Namely, I use the Volkov central force [59] with the Bartlett, Heisenberg, and Majorana parameters  $b = h = 0.06$  and  $m = 0.60$  and the G3RS spin-orbit force [60] with the strength  $u_I = -u_{II} = 1300$  MeV, and the Coulomb force approximated by seven Gaussians. Using these interactions, Energies of  $^{10}\text{B}$  are obtained to be  $-54.3$  MeV for the ground state ( $3^+$ ) and  $-53.4$  MeV for the first excite state ( $1^+$ ) with the  $2\alpha + pn$  cluster model by superposing  $\sum_{I_z, d} \hat{P}_{MI_z}^{I\pi} \Phi_{^{10}\text{B}}(\mathbf{X}_B = 0; d, \phi = 0)$  with  $d = 1, 2$  (fm). Though the calculation underestimates the experimental binding energy (64.75 MeV), it reproduces the spin parity of the ground state ( $^{10}\text{B}(3_{\text{g.s.}}^+)$ ), and also the calculated excitation energy  $E_x = 0.9$  MeV of the  $1^+$  state reasonably agrees to the experimental value  $E_x = 0.72$  MeV for  $^{10}\text{B}(1_1^+)$ .

Using the  $^{10}\text{B}+\alpha$  cluster wave function in Eq. (8), I calculate positive-parity states of  $^{14}\text{N}$ . Properties of the ground state  $^{14}\text{N}(1_{\text{g.s.}}^+)$  are reasonably reproduced by the present calculation. Namely, the binding energy B.E.=102.6 MeV, the magnetic moment  $\mu = 0.36$  ( $\mu_N$ ), and the electric quadrupole moment  $Q = 2.4$  ( $\text{efm}^2$ ) of  $^{14}\text{N}(1_{\text{g.s.}}^+)$ , obtained by the present calculation reasonably agree to the experimental data (B.E.=104.66 MeV,  $\mu = 0.4038$  ( $\mu_N$ ), and  $Q = 1.93(8)$  ( $\text{efm}^2$ )). The calculated energy spectra are shown in Fig. 2. The  $\alpha$ -decay threshold is much higher

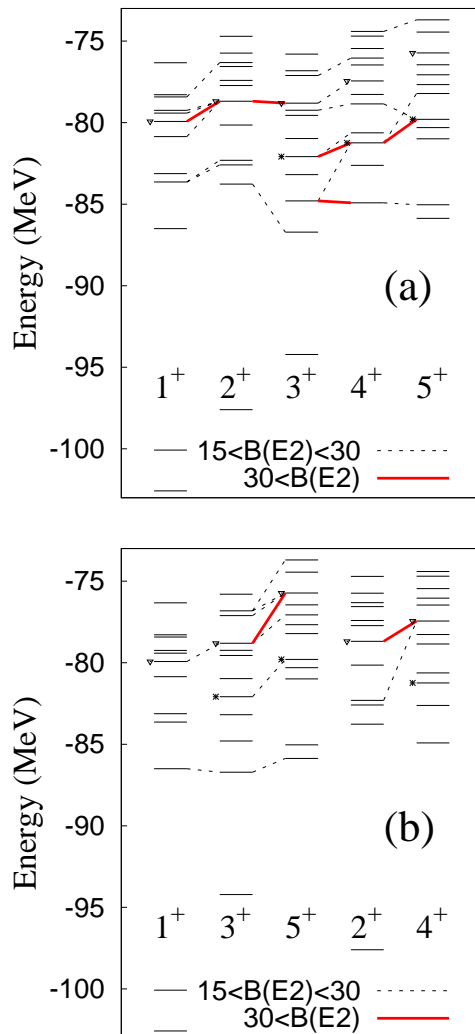


FIG. 3: (Color online)  $E2$  transition strengths calculated by the  $^{10}\text{B} + \alpha$  cluster model for (a)  $J^+ \rightarrow J^+ - 1$  and (b)  $J^+ \rightarrow J^+ - 2$  transitions with  $B(E2) \geq 15e^2\text{fm}^4$ . Asterisk and down-triangle symbols show  $^{10}\text{B} + \alpha$  cluster states in the  $K^\pi = 3^+$  and  $K^\pi = 1^+$  bands, respectively.

in the present calculation than the experimental threshold. In other words, the ground and some low-lying states of  $^{14}\text{N}$  show too deep binding from the  $\alpha$ -decay threshold compared with the experimental data. The significant overestimation of the  $\alpha$ -decay threshold is a general problem in microscopic calculations with density-independent two-body effective interactions as found for  $^{14}\text{C}$  and O isotopes [6, 32, 54]. One of the origins of this problem is a difficulty in reproducing systematics of binding energies in a wide mass-number region with such effective interactions. In this paper, I mainly investigate  $^{10}\text{B} + \alpha$  cluster states near the  $\alpha$ -decay threshold and discuss their features. In the calculated energy levels near the threshold, I obtain several excited states having significant component of a spatially developed  $\alpha$  cluster around the  $^{10}\text{B}$  cluster. From remarkable  $E2$  transitions, I assign the  $^{10}\text{B} + \alpha$  cluster states to a  $K^\pi = 3^+$  band of  $J^\pi = 3^+$ ,  $4^+$ , and  $5^+$  states, and a  $K^\pi = 1^+$  band of  $J^\pi = 1^+$ ,  $2^+$ ,  $3^+$ ,  $4^+$ , and  $5^+$  states. The former and the latter bands are shown by asterisk and down-triangle symbols in Fig. 2. The  $K^\pi = 3^+$  band has the significant  $^{10}\text{B}(3^+) + \alpha$  component, whereas the  $K^\pi = 1^+$  band contains the  $^{10}\text{B}(1^+) + \alpha$  component. More details of structure of these states are discussed in the next section.

Figure 3 shows  $E2$  transitions with  $B(E2) \geq 15 e^2\text{fm}^4$  for  $J \rightarrow J - 1$  and  $J \rightarrow J - 2$  transitions. In-band transitions for the  $K^\pi = 3^+$  and  $\pi = 1^+$   $^{10}\text{B} + \alpha$  bands are rather strong because of the developed cluster structures, though  $E2$  strengths are somewhat fragmented into neighboring states.

## IV. DISCUSSION

$^{10}\text{B}+\alpha$  cluster states in the  $K^\pi = 3^+$  and  $K^\pi = 1^+$  bands have maximum amplitudes of  $\alpha$ -cluster probability around  $D_\alpha = 5$  fm. In this section, I focus on angular motion of the  $\alpha$  cluster at  $D_\alpha = 5$  fm. I first investigate the angular momentum coupling of the  $\alpha$ -cluster ( $L_\alpha$ ) and the  $^{10}\text{B}$  cluster ( $I$ ) in a weak coupling picture and estimate  $\alpha$ -decay widths. Then, I discuss geometric configurations of  $^{10}\text{B}+\alpha$  cluster states in the strong coupling picture by analyzing  $\theta_\alpha$ -dependence of the  $\alpha$ -cluster probability around the deformed  $^{10}\text{B}$  cluster.

### A. $D_\alpha$ -fixed calculation

In the present calculation, radial motion of the  $\alpha$  cluster is described by superposing  $^{10}\text{B}+\alpha$  wave functions for  $D_\alpha = 2, \dots, 6$  fm. Instead of the full model space in Eq. (8) including  $D_\alpha = 2, \dots, 6$  fm wave functions, I also perform a similar calculation using the  $D_\alpha$ -fixed model space

$$\Psi_{^{14}\text{N}(J_\pi)}^{D_\alpha=5} = \sum_K \sum_{\theta_\alpha} \sum_{d,\phi} C(K, \theta_\alpha, d, \phi) \hat{P}_{MK}^{J_\pi} \Phi_{^{10}\text{B}+\alpha}(D_\alpha, \theta_\alpha; d, \phi), \quad (14)$$

where I fix  $D_\alpha = 5$  fm and take  $\theta_\alpha = \{0, \pi/8, \pi/4, 3\pi/8, \pi/2\}$ ,  $d = \{1, 2\}$  (fm), and  $\phi = \frac{\pi}{4}(j - 0.5)$  ( $j = 1, \dots, 8$ ). In the  $D_\alpha = 5$  fm fixed calculation, I find the states near the threshold energy corresponding to  $^{10}\text{B}+\alpha$  cluster states in the  $K^\pi = 3^+$  and  $K^\pi = 1^+$  bands, but do not obtain lower states below the threshold because of the truncation of the model space. Energy levels of the  $K^\pi = 3^+$  and  $K^\pi = 1^+$  bands obtained with the full and  $D_\alpha$ -fixed calculations are shown in Fig. 4. The calculated energies are measured from the  $\alpha$ -decay threshold. The experimental levels observed by  $\alpha$  elastic scattering by  $^{10}\text{B}$  are also shown in the figure. The level structures of the  $K^\pi = 3^+$  and  $K^\pi = 1^+$  bands are essentially consistent between the full and  $D_\alpha$ -fixed calculations, though about 2 MeV global shift is found for the  $K^\pi = 3^+$  band between two calculations.

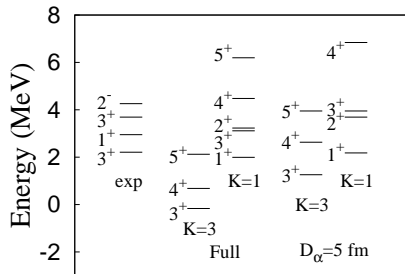


FIG. 4: Energies of  $^{10}\text{B}+\alpha$  cluster states obtained by the full and  $D_\alpha$ -fixed calculations and those observed by the experiment of  $^{10}\text{B}(\alpha, \alpha)^{10}\text{B}$  reactions [57]. Energies are measured from the  $\alpha$ -decay threshold.

### B. $\alpha$ -cluster probability and $\alpha$ -decay widths

In Table I, I show  $L_\alpha$  components ( $P_{^{10}\text{B}(I^\pi) \otimes L_\alpha}$  in Eq. (11)) at  $D_\alpha = 5$  fm coupled with  $^{10}\text{B}(3^+)$  and  $^{10}\text{B}(1^+)$  in  $^{10}\text{B}+\alpha$  cluster states obtained by the full and  $D_\alpha$ -fixed calculations. In the result of the  $D_\alpha$ -fixed calculation,  $K^\pi = 3^+$  band states are dominated by the  $^{10}\text{B}(3^+) \otimes L_\alpha$  component, whereas  $K^\pi = 1^+$  band states contain dominantly the  $^{10}\text{B}(1^+) \otimes L_\alpha$  component. In the result of the full calculation, the  $K^\pi = 3^+$  and  $K^\pi = 1^+$  band states still contain significant  $^{10}\text{B}(3^+) \otimes L_\alpha$  and  $^{10}\text{B}(1^+) \otimes L_\alpha$  components, respectively, except for the  $1^+(K^\pi = 1^+)$  state, though the absolute amplitude of the dominant component decreases because of radial motion and state mixing. The  $1^+(K^\pi = 1^+)$  state obtained by the full calculation shows a feature quite different from that obtained by the  $D_\alpha$ -fixed calculation. In the  $D_\alpha$ -fixed calculation, the  $1^+(K^\pi = 1^+)$  state is approximately described by the pure  $^{10}\text{B}(1^+) \otimes (L_\alpha = 0)$  state, where the orbital angular momentum ( $L_\alpha$ ) of the  $\alpha$  cluster weakly couples to the spin ( $I$ ) of the  $^{10}\text{B}$  cluster. However, in the full calculation, the  $1^+(K^\pi = 1^+)$  state does not show the weak coupling feature but has  $^{10}\text{B}(1^+) \otimes (L_\alpha = 0)$ ,  $^{10}\text{B}(1^+) \otimes (L_\alpha = 2)$ , and  $^{10}\text{B}(3^+) \otimes (L_\alpha = 2)$  components with the same order showing a strong coupling feature.

Figure 5 shows  $L_\alpha$  components ( $P_{10B(I^\pi) \otimes L_\alpha}$ ) at  $D_\alpha = 5$  fm of  $J^\pi$  states in the  $^{14}\text{N}$  spectra obtained by the full calculation. The  $^{10}\text{B}(3^+) + (L_\alpha = 0)$  and  $^{10}\text{B}(3^+) + (L_\alpha = 2)$  components concentrate at the  $3^+(K^\pi = 3^+)$  and  $4^+(K^\pi = 3^+)$  states, respectively, though the components are fragmented into other states. The  $5^+(K^\pi = 3^+)$  state shows rather strong state mixing. The  $^{10}\text{B}(1^+) + (L_\alpha = 2)$  component concentrates at the  $2^+(K^\pi = 1^+)$  and  $3^+(K^\pi = 1^+)$  states, whereas, the  $^{10}\text{B}(1^+) + (L_\alpha = 0)$  component feeds lower  $1^+$  states of  $^{14}\text{N}$ .

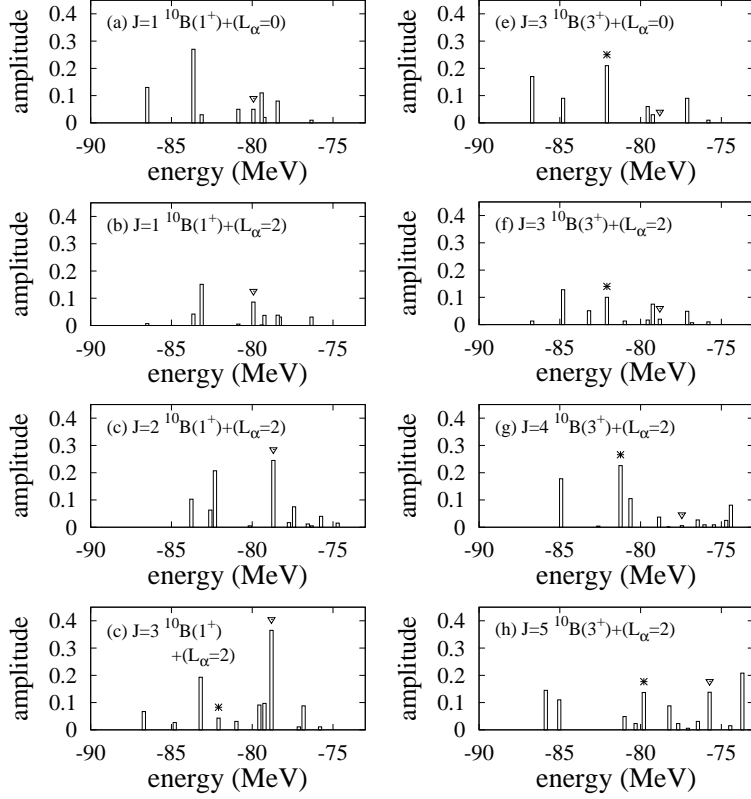


FIG. 5:  $^{10}\text{B}(I^\pi) \otimes (L_\alpha = 0, 2)$  components,  $P_{10B(I^\pi) \otimes L_\alpha}(D_\alpha = 5\text{fm})$ , in positive-parity states of  $^{14}\text{N}$  obtained by the  $^{10}\text{B} + \alpha$ -cluster model. Asterisk and down-triangle symbols show  $^{10}\text{B} + \alpha$  cluster states in the  $K^\pi = 3^+$  and  $K^\pi = 1^+$  bands, respectively.

In the experiment of  $^{10}\text{B}(\alpha, \alpha)^{10}\text{B}$  reactions [57], the  $3^+$  state at  $E_r = 1.58$  MeV ( $E_x = 13.19$  MeV) with the width  $\Gamma = 0.065$  MeV is strongly populated. In the analysis of Ref. [57], this state is described well by the dominant (almost 100%)  $S$ -wave  $\alpha$ -decay indicating the significant  $^{10}\text{B}(3^+) \otimes (L_\alpha = 0)$  component of the  $3^+$  state. The  $1^+$  state at  $E_r = 2.11$  MeV ( $E_x = 13.72$  MeV) is weakly populated in  $^{10}\text{B}(\alpha, \alpha)^{10}\text{B}$  reactions, whereas its  $\alpha$ -decay into the first excited state of  $^{10}\text{B}(1^+)$  was observed in  $^{10}\text{B}(\alpha, \alpha')^{10}\text{B}$  reactions [62]. These experiments suggest that the  $1^+$  state would contain  $^{10}\text{B}(1^+) \otimes (L_\alpha = 0)$  and  $^{10}\text{B}(3^+) \otimes (L_\alpha = 2)$  components.

From the experimental  $\alpha$ -decay properties, I tentatively assign the theoretical  $3^+(K^\pi = 3^+)$  and  $1^+(K^\pi = 1^+)$  states having  $^{10}\text{B} + \alpha$  cluster structures to the experimental  $3^+$  ( $E_r^{\text{exp}} = 1.58$  MeV) and  $1^+$  ( $E_r^{\text{exp}} = 2.11$  MeV) states, though the band-head energies  $E_r(3^+; K^\pi = 3^+) = -0.2$  MeV and  $E_r(1^+; K^\pi = 1^+) = 2.0$  MeV obtained by the full calculation do not necessarily agree to the experimental energies (see Fig. 4). I estimate partial  $\alpha$ -decay widths for  $B(I^\pi) \otimes L_\alpha$  channels from  $P_{10B(I^\pi) \otimes L_\alpha}(D_\alpha = a)$  ( $a$  is the channel radius) as follows. Using the approximate evaluation of the reduced width amplitude proposed in Ref. [63], the reduced width  $\gamma_\alpha^2(a)$  is calculated as

$$\gamma_\alpha^2(a) = \frac{\hbar^2}{2\mu a} \left( \frac{\nu}{2\pi} \frac{A_1 A_2}{A_1 + A_2} \right)^{1/2} P_{10B(I^\pi) \otimes L_\alpha}(D_\alpha = a), \quad (15)$$

and the partial  $\alpha$ -decay width  $\Gamma_{10B(I^\pi) + \alpha}$  for  $L_\alpha = l$  is calculated as

$$\Gamma_{10B(I^\pi) + \alpha} = 2P_l(a)\gamma_\alpha^2(a), \quad (16)$$

$$P_l(a) = \frac{ka}{F_l^2(ka) + G_l^2(ka)}, \quad (17)$$

where  $k = \sqrt{2\mu E}/\hbar$ , and  $F_l$  and  $G_l$  are the regular and irregular Coulomb functions, respectively. Here I use the momentum  $k$  of the energy  $E = E_r^{(\text{adjust})}$  which is phenomenologically adjusted to the experimental energy position because it is difficult to quantitatively predict the energy position in the present calculation. Namely, I adjust the band-head energies of the  $K^\pi = 3^+$  and  $K^\pi = 1^+$  bands to the experimental energy positions  $E_r^{\text{exp}}(3^+) = 1.58$  MeV and  $E_r^{\text{exp}}(1^+) = 2.11$  MeV, by a constant shift for each band as

$$E_r^{(\text{adjust})}(J^+; K^\pi = 3^+) = E_r(J^+; K^\pi = 3^+) - E_r(3^+; K^\pi = 3^+) + E_r^{\text{exp}}(3^+), \quad (18)$$

$$E_r^{(\text{adjust})}(J^+; K^\pi = 1^+) = E_r(J^+; K^\pi = 1^+) - E_r(1^+; K^\pi = 1^+) + E_r^{\text{exp}}(1^+). \quad (19)$$

Calculated partial  $\alpha$ -decay widths are shown in Table I. I calculate widths for  $L_\alpha = 0$  and  $L_\alpha = 2$  channels.  $\alpha$ -decay widths obtained by the full calculation are several times smaller than those obtained by the  $D_\alpha$ -fixed calculation because of the suppression of the  $\alpha$ -cluster probability as shown previously. As a result, the  $\alpha$ -decay width of the  $3^+(K^\pi = 3^+)$  state reduces to be  $\Gamma_\alpha = 0.05$  MeV with the dominant  $^{10}\text{B}(3^+) \otimes (L_\alpha = 0)$  decay, which is quantitatively consistent with the experimental observation ( $\Gamma_\alpha \sim \Gamma = 0.065(10)$  MeV) [57]. For the  $1^+(K^\pi = 1^+)$  state, I obtain a small  $\alpha$ -decay width  $\Gamma_\alpha = 0.01$  MeV with the dominant  $^{10}\text{B}(1^+) \otimes (L_\alpha = 0)$  decay. This result seems consistent with the weak population in the  $\alpha$  elastic scattering [57] and the fact that the  $1^+$  state was observed in  $^{10}\text{B}(\alpha, \alpha'\gamma)^{10}\text{B}$  reaction [62]. However, experimental information of partial  $\alpha$ -decay widths is not enough to confirm the present assignment of the  $1^+(K^\pi = 1^+)$  state. The calculated  $\alpha$ -decay width is much smaller than the experimental total width,  $\Gamma = 0.16(2)$  MeV, of the  $1^+$  state at 2.11 MeV. I should comment that, because the  $^{10}\text{B}(1^+) \otimes (L_\alpha = 0)$  component is fragmented into neighboring states as shown in Fig. 5, an effectively large width could be observed for the  $1^+(K^\pi = 1^+)$  state.

TABLE I:  $^{10}\text{B}(I^\pi) \otimes (L_\alpha = 0, 2)$  components,  $P_{^{10}\text{B}(I^\pi) \otimes L_\alpha}(D_\alpha = 5 \text{ fm})$ , of  $^{10}\text{B} + \alpha$  cluster states in the  $K^\pi = 3^+$  and  $K^\pi = 1^+$  bands obtained by the full and  $D_\alpha$ -fixed calculations.

$J^\pi$	$P_{^{10}\text{B}(3^+) \otimes L_\alpha}$		$P_{^{10}\text{B}(1^+) \otimes L_\alpha}$	
	$L_\alpha = 0$	$L_\alpha = 2$	$L_\alpha = 0$	$L_\alpha = 2$
full cal.				
$3^+(K^\pi = 3^+)$	0.21	0.10		0.04
$4^+(K^\pi = 3^+)$		0.23		
$5^+(K^\pi = 3^+)$		0.14		
$1^+(K^\pi = 1^+)$		0.03	0.05	0.09
$2^+(K^\pi = 1^+)$		0.02		0.25
$3^+(K^\pi = 1^+)$	0.00	0.02		0.37
$4^+(K^\pi = 1^+)$		0.01		
$5^+(K^\pi = 1^+)$		0.14		
$D_\alpha$ -fixed cal.				
$3^+(K^\pi = 3^+)$	0.57	0.25		0.01
$4^+(K^\pi = 3^+)$		0.73		
$5^+(K^\pi = 3^+)$		0.75		
$1^+(K^\pi = 1^+)$		0.02	0.89	0.05
$2^+(K^\pi = 1^+)$		0.01		0.78
$3^+(K^\pi = 1^+)$	0.10	0.13		0.74
$4^+(K^\pi = 1^+)$		0.00		

### C. Angular motion of the $\alpha$ cluster around the deformed $^{10}\text{B}$ cluster

I here discuss angular motion of the  $\alpha$ -cluster around the deformed  $^{10}\text{B}$  cluster by analyzing  $\theta_\alpha$  dependence of  $\alpha$ -cluster probabilities. Discussions in this section are based on the strong coupling picture, which is somehow different from the previous discussion based on the  $L_\alpha$  decomposition in the weak coupling picture. I show energies of  $\Phi_{^{10}\text{B}(I_z^\pi) + \alpha}(D_\alpha, \theta_\alpha)$ , in which the  $\alpha$  cluster is localized at  $(D_\alpha, \theta_\alpha)$  around the  $I_z$  projected  $^{10}\text{B}$  cluster. In Fig. 5, intrinsic energies before parity and angular-momentum projections of  $\Phi_{^{10}\text{B}(I_z^\pi) + \alpha}(D_\alpha, \theta_\alpha)$  for  $I_z^\pi = 3^+$  and  $1^+$  are



TABLE II: Partial  $\alpha$ -decay widths of  $^{10}\text{B}+\alpha$  cluster states in the  $K^\pi = 3^+$  and  $K^\pi = 1^+$  bands obtained by the full and  $D_\alpha$ -fixed calculations. Energies of the band-head states of the  $K^\pi = 3^+$  and  $K^\pi = 1^+$  bands are adjusted to the experimental resonance energies of the  $3^+$  state at 1.58 MeV and the  $1^+$  state at 2.11 MeV. The sum ( $\Gamma_{^{10}\text{B}+\alpha}(L_\alpha \leq 2)$ ) of partial widths of decay channels  $^{10}\text{B}(3^+) \otimes (L_\alpha \leq 2)$  and  $^{10}\text{B}(1^+) \otimes (L_\alpha \leq 2)$  is also shown. The unit is MeV.

$J^\pi$	$E_r^{(\text{adjust})}$	$\Gamma_{^{10}\text{B}(3^+)+\alpha}$		$\Gamma_{^{10}\text{B}(1^+)+\alpha}$		$\Gamma_{^{10}\text{B}(3^+)+\alpha}(L_\alpha \leq 2)$
		$L_\alpha = 0$	$L_\alpha = 2$	$L_\alpha = 0$	$L_\alpha = 2$	
full cal.						
$3^+(K^\pi = 3^+)$	1.58	0.04	0.00		0.00	0.05
$4^+(K^\pi = 3^+)$	2.43		0.06			0.06
$5^+(K^\pi = 3^+)$	3.87		0.16			0.16
$1^+(K^\pi = 1^+)$	2.11		0.00	0.01	0.00	0.01
$2^+(K^\pi = 1^+)$	3.35		0.02		0.09	0.11
$3^+(K^\pi = 1^+)$	3.23	0.00	0.01		0.12	0.13
$4^+(K^\pi = 1^+)$	4.60		0.01			0.01
$5^+(K^\pi = 1^+)$	6.31		0.36			0.36
$D_\alpha$ -fixed cal.						
$3^+(K^\pi = 3^+)$	1.58	0.12	0.01		0.00	0.13
$4^+(K^\pi = 3^+)$	2.95		0.41			0.41
$5^+(K^\pi = 3^+)$	4.27		1.07			1.07
$1^+(K^\pi = 1^+)$	2.11		0.00	0.10	0.00	0.11
$2^+(K^\pi = 1^+)$	3.61		0.01		0.41	0.42
$3^+(K^\pi = 1^+)$	3.88	0.19	0.15		0.51	0.85
$4^+(K^\pi = 1^+)$	6.77		0.01			0.01

plotted on the  $(x, z) = (D_\alpha \sin \theta_\alpha, D_\alpha \cos \theta_\alpha)$  plane. The energy curves for  $D_\alpha = 5$  fm are also shown as functions of  $\theta_\alpha$ . In the  $D_\alpha \geq 5$  fm region, the contour of the energy surface on the  $(x, z)$  plane is deformed in the longitudinal ( $\theta_\alpha = 0$ ) direction because of the prolate deformation of the  $^{10}\text{B}$  cluster meaning that the  $\alpha$  cluster at the fixed distance  $D_\alpha = 5$  fm feels an attraction in the longitudinal direction. In other words, in the intrinsic system, the  $\alpha$  cluster at  $D_\alpha = 5$  fm energetically favors the longitudinal direction to form the linear  $3\alpha$  configuration rather than the transverse direction to form the triangle  $3\alpha$  configuration. In the  $D_\alpha \leq 3$  fm region, the  $\alpha$  cluster feels an effective repulsion in the longitudinal direction because of the Pauli blocking from the  $^{10}\text{B}$  cluster, whereas it feels an attraction in the transverse ( $\theta_\alpha = \pi/2$ ) direction.

In contrast to the intrinsic energy behavior,  $\theta_\alpha$  dependence of  $J^\pi$ -projected energy is not trivial because the energy is affected by not only potential energy but also kinetic energy of angular motion, i.e., rotational energy. Figure 7 shows energies of  $JK$ -projected states  $\hat{P}_{MK}^{J^\pi} \Phi_{^{10}\text{B}(I_z)+\alpha}(D_\alpha, \theta_\alpha)$  at  $D_\alpha = 5$  fm for  $K = I_z$ , which corresponds to the  $L_{\alpha z} = 0$  projection. In high  $J$  states, the longitudinal direction ( $|\theta_\alpha| \lesssim \pi/8$ ) is energetically favored than the transverse direction ( $|\theta_\alpha - \pi/2| \lesssim \pi/8$ ) because of the larger moment of inertia (m.o.i.) of the longitudinal configuration than that of the transverse configuration for the  $L_{\alpha z} = 0$  projection. However, in the lowest spin state ( $JK = 11$ ), the energy almost degenerates in a wide region of  $\theta_\alpha$  because the kinetic energy is smaller for the transverse configuration than the longitudinal configuration because of the phase space factor  $\sin \theta_\alpha$  in the  $L_{\alpha z} = 0$  projection. This energy degeneracy results in the  $L_\alpha = 0$  ( $S$ -wave) dominance in the  $1^+(K^\pi = 1^+)$  state obtained by the  $D_\alpha$ -fixed calculation.

Figures 8 and 9 show energies of  $JK$ -projected states at  $D_\alpha = 5$  fm for  $K \neq I_z$ . Note that the  $K \neq I_z$  projection corresponds to the  $L_{\alpha z} \neq 0$  projection, and  $K > I_z$  means the  $L_\alpha$  alignment to the  $z$  direction (see Fig. 1(c)). For instance, the  $L_\alpha$ -aligned state for  $L_\alpha = 2$  ( $D$ -wave) is the  $K = I_z + 2$  state. As shown in Figs. 8(a)-(c) and 9(a)-(d),  $L_\alpha$ -aligned states energetically favor the transverse configuration because of the larger m.o.i. than that of the longitudinal configuration in the  $L_{\alpha z} = 2$  projection. Figures 8 and 9 also show the  $\alpha$ -cluster probability  $P(JK; ^{10}\text{B}(I_z^\pi); D_\alpha, \theta_\alpha)$  at  $D_\alpha = 5$  fm in the  $^{10}\text{B}+\alpha$  cluster states obtained by the  $D_\alpha$ -fixed and full calculations. Let me first discuss the result obtained by the  $D_\alpha$ -fixed calculation (Figs. 8(d)-(f) and 9(e)-(h)). In the  $K^\pi = 3^+$  band states (Fig. 8(d)-(f)), the  $J^\pi = 3^+$  state contains dominantly the longitudinal configuration ( $|\theta_\alpha| \lesssim \pi/8$ ) rather than the transverse configuration ( $|\theta_\alpha - \pi/2| \lesssim \pi/8$ ) as expected from the  $JK$ -projected energy curve for  $K = I_z$ . As  $J$  goes up to  $J = 5$ , the  $L_\alpha$ -aligned component ( $K = 5$ ) of the transverse configuration becomes large corresponding to the alignment of the orbital angular momentum  $L_\alpha$  of the  $\alpha$  cluster to  $I_z = 3$  (the spin of  $(pn)$  cluster in the  $^{10}\text{B}$  cluster). In the  $K^\pi = 1^+$  band states (Fig. 9(e)-(h)), the  $J^\pi = 1^+$  state shows the  $\alpha$ -cluster probability distributed widely

in the  $0 \leq \theta_\alpha \leq \pi/2$  region indicating the dominant  $L_\alpha = 0$  ( $S$ -wave) component. As  $J$  increases, the longitudinal component becomes dominant compared with the transverse component. The alignment of  $L_\alpha$  (the orbital angular momentum of the  $\alpha$  cluster) and  $I_z$  is not so remarkable for  $^{10}\text{B}(I_z^\pi = 1^+)$  differently from the  $^{10}\text{B}(I_z^\pi = 3^+)$ . Next, let me look into the result of the full calculation shown in Figs. 8(g)-(i) and 9(i)-(l). Compared with the  $D_\alpha$ -fixed calculation, transverse components tend to be relatively more suppressed than longitudinal components in the full calculation. Note that the longitudinal ( $\theta_\alpha = 0$ ) component is not dominant but is  $30 \sim 40\%$ , which is comparable to the  $\theta_\alpha = \pi/4$  component. It indicates that  $^{10}\text{B}+\alpha$  cluster states are different from the ideal linear configuration of a classical picture but they show significant quantum fluctuation in the angular ( $\theta_\alpha$ ) motion and are regarded as the chain-like configuration that has relatively enhanced longitudinal components with suppressed transverse components.

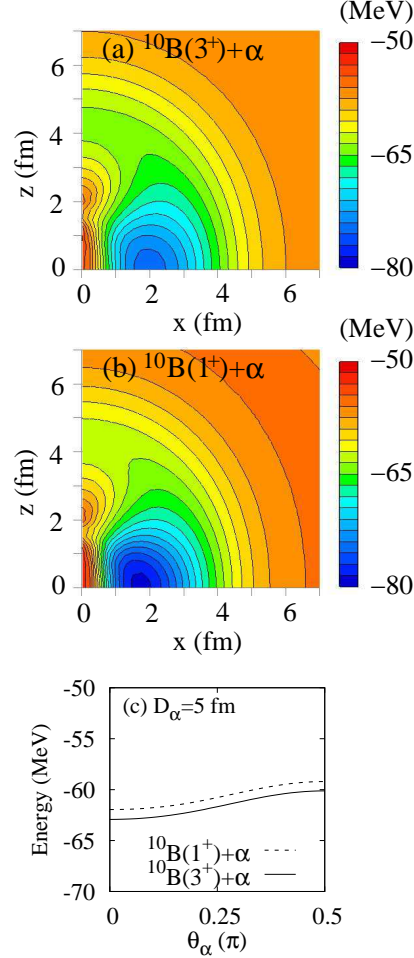


FIG. 6: Intrinsic energies of  $^{10}\text{B}(I_z^\pi = 3^+) + \alpha$  and  $^{10}\text{B}(I_z^\pi = 1^+) + \alpha$  before the parity and angular-momentum projections. Energies for (a)  $^{10}\text{B}(I_z^\pi = 3^+) + \alpha$  and (b)  $^{10}\text{B}(I_z^\pi = 1^+) + \alpha$  plotted on  $(x, z) = (D_\alpha \sin \theta_\alpha, D_\alpha \cos \theta_\alpha)$ , and (c) those at  $D_\alpha = 5$  fm plotted as functions of  $\theta_\alpha$ .

The origin of the suppression of transverse components in  $^{10}\text{B}+\alpha$  cluster states in the full calculation can be described by orthogonality to lower states which contain transverse components with  $D_\alpha < 5$  fm. As shown in Fig. 6 for the energy surface on the  $(D_\alpha, \theta_\alpha)$  plane, an energy pocket exists in the transverse direction ( $\theta_\alpha \sim \pi/2$ ) around  $D_\alpha \sim 2$ , and therefore, transverse components contribute to low-lying  $^{14}\text{N}$  states. Although the low-lying states are compact states containing mainly configurations with small  $D_\alpha$ , transverse components with  $D_\alpha = 5$  fm somewhat feed the low-lying states. As a result of the feeding of lower states, transverse components in the  $^{10}\text{B}+\alpha$  cluster states near the threshold are suppressed. Figures 10 and 11 show the  $\alpha$ -cluster probability  $P(JK; ^{10}\text{B}(I_z^\pi); D_\alpha, \theta_\alpha)$  for  $\theta_\alpha = 0$  at  $D_\alpha = 5$  fm and that for  $\theta_\alpha = \pi/4$  and  $\pi/2$  at  $D_\alpha = 4$  fm. As seen in 10(a)-(c) for  $^{10}\text{B}(I_z^\pi = 3^+) + \alpha$ , the longitudinal ( $\theta_\alpha = 0$ ) component of  $^{10}\text{B}(I_z^\pi = 3^+) + \alpha$  shows the largest amplitude at the  $K^\pi = 3^+$  band states (labeled by asterisks) and some fragmentation into neighboring states. Similarly, the longitudinal component of  $^{10}\text{B}(I_z^\pi = 1^+) + \alpha$

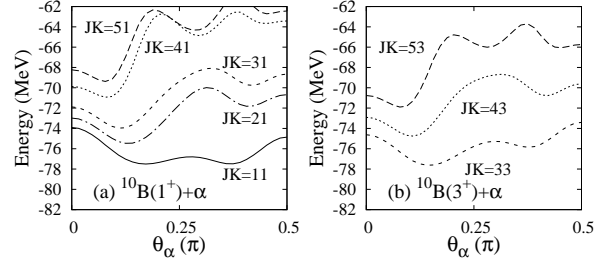


FIG. 7: Energies of the  $JK$ -projected  $\Phi_{^{10}\text{B}(I_z^\pi)+\alpha}$  wave function  $\hat{P}_{MK}^{J\pi}\Phi_{^{10}\text{B}(I_z^\pi)+\alpha}(D_\alpha, \theta_\alpha)$  with  $K = I_z$  for (a)  $^{10}\text{B}(I_z^\pi = 3^+)$  and (b)  $^{10}\text{B}(I_z^\pi = 1^+)$ . Energies for  $D_\alpha = 5$  fm are plotted as functions of  $\theta_\alpha$ .

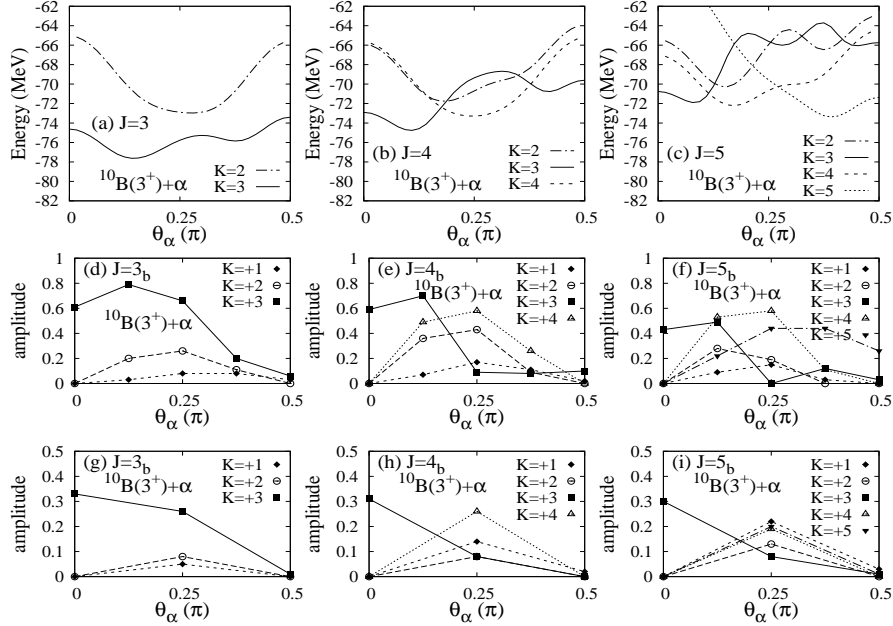


FIG. 8: (a)(b)(c) Energies of the  $JK$ -projected  $\Phi_{^{10}\text{B}(I_z^\pi)+\alpha}$  wave function  $\hat{P}_{MK}^{J\pi}\Phi_{^{10}\text{B}(I_z^\pi)+\alpha}(D_\alpha, \theta_\alpha)$  for  $^{10}\text{B}(I_z^\pi = 3^+)$ . (d)(e)(f)  $\alpha$ -cluster probability  $P(JK; ^{10}\text{B}(I_z^\pi); D_\alpha, \theta_\alpha)$  for  $I_z^\pi = 3^+$  at  $D_\alpha = 5$  fm in  $K^\pi = 3^+$   $^{10}\text{B} + \alpha$  cluster states obtained by the  $D_\alpha$ -fixed calculation and (g)(h)(i) that obtained by the full calculation.

concentrates on the  $K^\pi = 1^+$  band states (see Fig. 11(a)-(e)). On the other hand, transverse components feed states lower than  $^{10}\text{B} + \alpha$ -cluster states as seen in Fig. 10(d)(f) and Fig. 11(f)(g)). Consequently the  $\alpha$  cluster in  $^{10}\text{B} + \alpha$ -cluster states near the threshold tends to avoid transverse configurations so as to satisfy orthogonality to lower states. This mechanism is consistent with the discussion of Ref. [54] for linear-chain  $3\alpha$  states in  $^{14}\text{C}$ .

## V. SUMMARY

I calculated positive-parity states of  $^{14}\text{N}$  with the  $^{10}\text{B} + \alpha$  cluster model and investigated  $^{10}\text{B} + \alpha$  cluster states. Near the  $\alpha$ -decay threshold energy, I obtained the  $K^\pi = 3^+$  and  $K^\pi = 1^+$  rotational bands having the developed  $\alpha$  cluster with the  $^{10}\text{B}(3^+)$  and  $^{10}\text{B}(1^+)$  cores, respectively. I assigned the  $3^+(K^\pi = 3^+)$  state in the present result to the experimental  $3^+$  at  $E_r = 1.58$  MeV observed in  $\alpha$  scattering reactions by  $^{10}\text{B}$ , and showed that the calculated  $\alpha$ -decay width agrees to the experimental width.

I analyzed the component of the longitudinal configuration having an  $\alpha$  cluster in the longitudinal direction of the deformed  $^{10}\text{B}$  cluster, which corresponds to a linear-chain  $3\alpha$  structure with valence nucleons. In the spectra

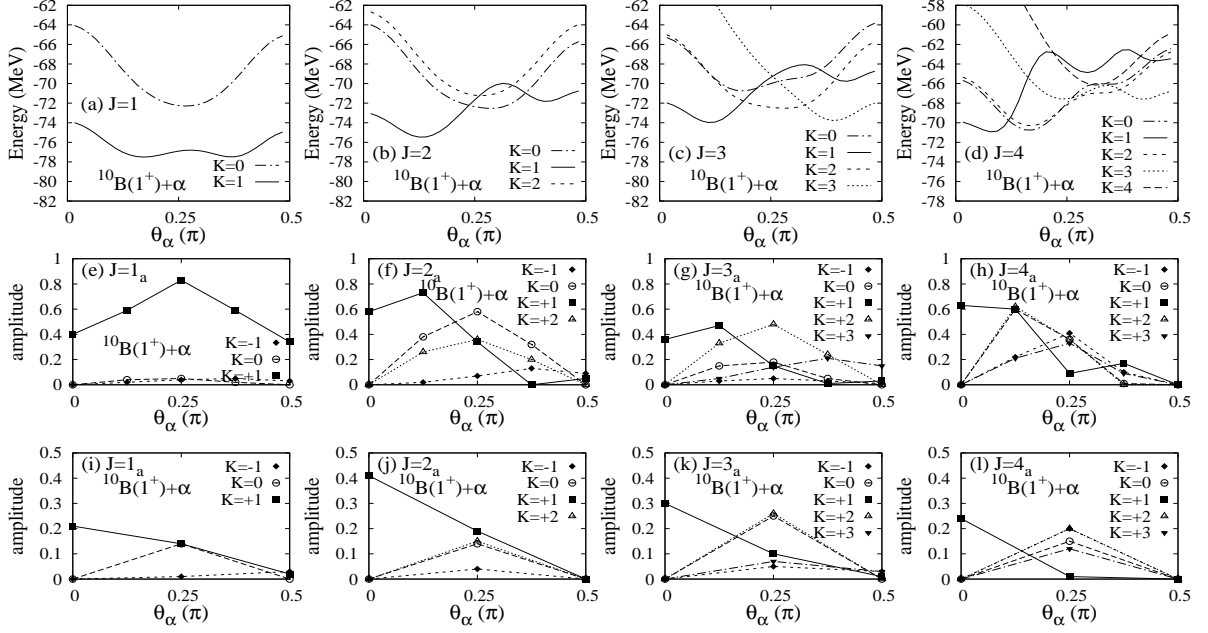


FIG. 9: (a)-(d) Energies of the  $JK$ -projected  $\Phi_{10\text{B}(I_z^\pi)+\alpha}$  wave function  $\hat{P}_{MK}^{J\pi} \Phi_{10\text{B}(I_z^\pi)+\alpha}(D_\alpha, \theta_\alpha)$  for  $^{10}\text{B}(I_z^\pi = 1^+)$ . (e)-(h)  $\alpha$ -cluster probability  $P(JK; ^{10}\text{B}(I_z^\pi); D_\alpha, \theta_\alpha)$  for  $I_z^\pi = 1^+$  at  $D_\alpha = 5$  fm in the  $K^\pi = 1^+$   $^{10}\text{B}+\alpha$  cluster states obtained by the  $D_\alpha$ -fixed calculation and (i)-(l) that obtained by the full calculation.

of  $^{14}\text{N}$ , the linear-chain component concentrates at the  $^{10}\text{B}+\alpha$  cluster states in the  $K^\pi = 3^+$  and  $K^\pi = 1^+$  bands. However, the  $^{10}\text{B}+\alpha$  cluster states are different from the ideal linear configuration of a classical picture but they show significant quantum fluctuation in the angular ( $\theta_\alpha$ ) motion and are regarded as the chain-like configuration that has relatively enhanced longitudinal components and suppressed transverse components. The orthogonality to low-lying states plays an essential role in the suppression of the transverse component.

### Acknowledgments

The authors would like to thank Dr. Suhara for fruitful discussions. The computational calculations of this work were performed by using the supercomputers at YITP. This work was supported by JSPS KAKENHI Grant Number 26400270.

- 
- [1] W. von Oertzen, M. Freer and Y. Kanada-En'yo, Phys. Rep. **432**, 43 (2006).
  - [2] Y. Kanada-En'yo and H. Horiuchi, Prog. Theor. Phys. Suppl. **142**, 205 (2001).
  - [3] Y. Kanada-En'yo M. Kimura and H. Horiuchi, C. R. Physique **4**, 497 (2003).
  - [4] Y. Kanada-En'yo, M. Kimura and A. Ono, PTEP **2012** 01A202 (2012).
  - [5] H. Horiuchi, K. Ikeda, and K. Katō, Prog. Theor. Phys. Suppl. **192**, 1 (2012).
  - [6] Y. Fujiwara *et al.*, Prog. Theor. Phys. Suppl. **68**, 29 (1980).
  - [7] M. Seya, M. Kohno, and S. Nagata, Prog. Theor. Phys. **65**, 204 (1981).
  - [8] W. von Oertzen, Z. Phys. A **354**, 37 (1996); **357**, 355 (1997); W. von Oertzen, Nuovo Cimento **110**, 895 (1997).
  - [9] K. Arai, Y. Ogawa, Y. Suzuki and K. Varga, Phys. Rev. C **54**, 132 (1996).
  - [10] A. Dote, H. Horiuchi and Y. Kanada-En'yo, Phys. Rev. C **56**, 1844 (1997).
  - [11] Y. Kanada-En'yo, H. Horiuchi and A. Doté, Phys. Rev. C **60**, 064304 (1999).
  - [12] N. Itagaki and S. Okabe, Phys. Rev. C **61**, 044306 (2000).
  - [13] Y. Ogawa, K. Arai, Y. Suzuki and K. Varga, Nucl. Phys. **A673**, 122 (2000).
  - [14] Y. Kanada-En'yo, Phys. Rev. C **66**, 011303 (2002).
  - [15] P. Descouvemont, Nucl. Phys. A **699**, 463 (2002).

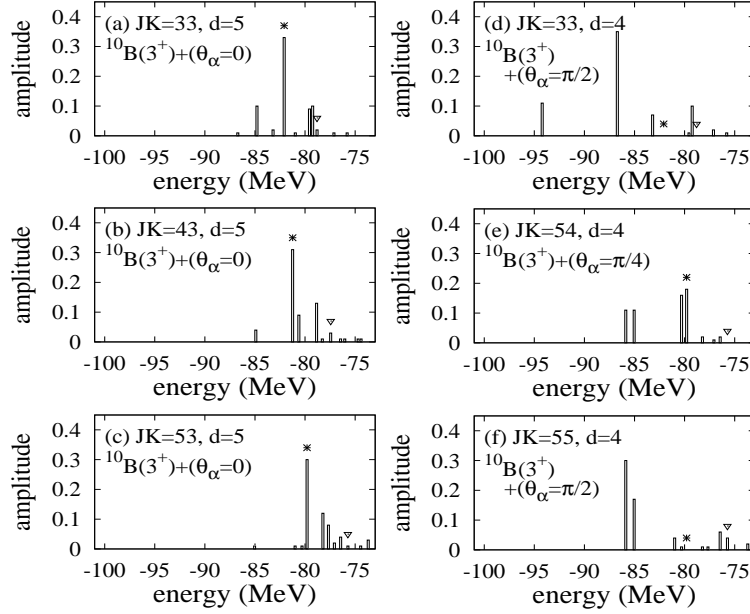


FIG. 10:  $\alpha$ -cluster probability  $P(JK; ^{10}\text{B}(I_z^\pi); D_\alpha, \theta_\alpha)$  for  $I_z^\pi = 3^+$ .  $D_\alpha$  is taken to be  $D_\alpha = 5$  fm for  $\theta_\alpha = 0$ , and  $D_\alpha = 4$  fm for  $\theta_\alpha = \pi/4$  and  $\pi/2$ . Asterisk and down-triangle symbols show  $^{10}\text{B} + \alpha$  cluster states in the  $K^\pi = 3^+$  and  $K^\pi = 1^+$  bands, respectively.

- [16] M. Ito, K. Kato and K. Ikeda, Phys. Lett. B **588**, 43 (2004).  
 [17] M. Ito, Phys. Lett. B **636**, 293 (2006).  
 [18] M. Freer *et al.*, Phys. Rev. Lett. **82**, 1383 (1999).  
 [19] M. Freer *et al.*, Phys. Rev. C **63**, 034301 (2001).  
 [20] A. Saito, *et al.*, Nucl. Phys. **A738**, 337 (2004); A. Saito *et al.*, Mod. Phys. Lett. A **25**, 1858 (2010).  
 [21] N. Curtis *et al.*, Phys. Rev. C **70**, 014305 (2004).  
 [22] M. Milin *et al.*, Nucl. Phys. **A753**, 263 (2005).  
 [23] M. Freer *et al.*, Phys. Rev. Lett. **96**, 042501 (2006).  
 [24] H. G. Bohlen, T. Dorsch, T. Kokalova, W. von Oertzen, C. Schulz and C. Wheldon, Phys. Rev. C **75**, 054604 (2007).  
 [25] N. Curtis *et al.*, J. Phys. G **36**, 015108 (2009).  
 [26] Z. H. Yang *et al.*, Phys. Rev. Lett. **112**, 162501 (2014).  
 [27] N. Soic *et al.*, Phys. Rev. C **68**, 014321 (2003).  
 [28] W. von Oertzen *et al.*, Eur. Phys. J. A **21**, 193 (2004).  
 [29] D. L. Price *et al.*, Phys. Rev. C **75**, 014305 (2007).  
 [30] P. J. Haigh *et al.*, Phys. Rev. C **78**, 014319 (2008).  
 [31] M. Gai *et al.*, Phys. Rev. Lett. **50**, 239 (1983).  
 [32] P. Descouvemont and D. Baye, Phys. Rev. C **31**, 2274 (1985).  
 [33] M. Gai, R. Keddy, D. A. Bromley, J. W. Olness and E. K. Warburton, Phys. Rev. C **36**, 1256 (1987).  
 [34] N. Furutachi, S. Oryu, M. Kimura, A. Dote and Y. Kanada-En'yo, Prog. Theor. Phys. **119**, 403 (2008).  
 [35] C. Fu *et al.*, Phys. Rev. C **77**, 064314 (2008).  
 [36] E. D. Johnson *et al.*, Eur. Phys. J. A **42**, 135 (2009).  
 [37] W. von Oertzen *et al.*, Eur. Phys. J. A **43**, 17 (2010).  
 [38] N. Curtis *et al.*, Phys. Rev. C **66**, 024315 (2002).  
 [39] N. I. Ashwood *et al.*, J. Phys. G **32**, 463 (2006).  
 [40] S. Yildiz *et al.*, Phys. Rev. C **73**, 034601 (2006).  
 [41] W. Scholz, P. Neogy, K. Bethge and R. Middleton, Phys. Rev. C **6**, 893 (1972).  
 [42] P. Descouvemont, Phys. Rev. C **38**, 2397 (1988).  
 [43] G. V. Rogachev *et al.*, Phys. Rev. C **64**, 051302 (2001).  
 [44] V. Z. Goldberg *et al.*, Phys. Rev. C **69**, 024602 (2004).  
 [45] M. Kimura, Phys. Rev. C **75**, 034312 (2007).  
 [46] A. Tohsaki, H. Horiuchi, P. Schuck and G. Ropke, Phys. Rev. Lett. **87**, 192501 (2001).  
 [47] Y. Funaki, A. Tohsaki, H. Horiuchi, P. Schuck and G. Ropke, Phys. Rev. C **67**, 051306 (2003).  
 [48] T. Yamada and P. Schuck, Phys. Rev. C **69**, 024309 (2004).  
 [49] Y. Funaki, T. Yamada, H. Horiuchi, G. Ropke, P. Schuck and A. Tohsaki, Phys. Rev. Lett. **101**, 082502 (2008).

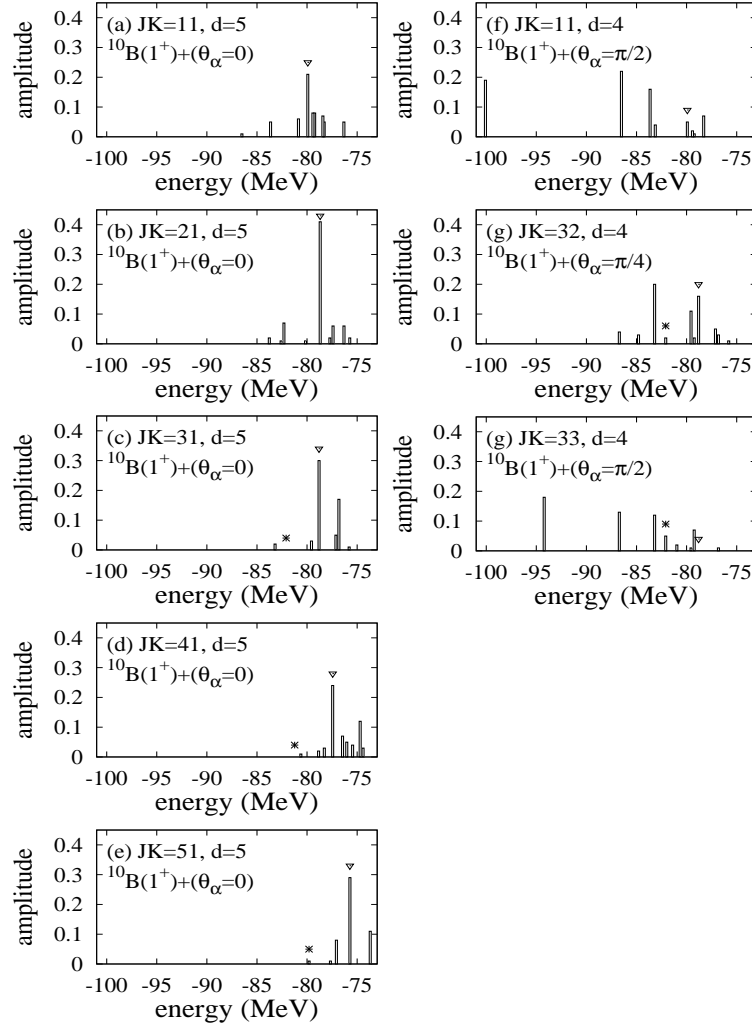


FIG. 11:  $\alpha$ -cluster probability  $P(JK; ^{10}\text{B}(I_z^\pi; D_\alpha, \theta_\alpha))$  for  $I_z^\pi = 1^+$ .  $D_\alpha$  is taken to be  $D_\alpha = 5$  fm for  $\theta_\alpha = 0$ , and  $D_\alpha = 4$  fm for  $\theta_\alpha = \pi/4$  and  $\pi/2$ . Asterisk and down-triangle symbols show  $^{10}\text{B}+\alpha$  cluster states in the  $K^\pi = 3^+$  band  $K^\pi = 1^+$  bands, respectively.

- [50] H. Morinaga, Phys. Rev. **101**, 254 (1956).
- [51] H. Morinaga, Phys. Lett. **21**, 78 (1966).
- [52] Y. Suzuki, H. Horiuchi and K. Ikeda, Prog. Theor. Phys. **47**, 1517 (1972).
- [53] N. Itagaki, S. Okabe, K. Ikeda and I. Tanihata, Phys. Rev. C **64**, 014301 (2001).
- [54] T. Suhara and Y. Kanada-En'yo, Phys. Rev. C **82**, 044301 (2010).
- [55] T. Ichikawa, J. A. Maruhn, N. Itagaki and S. Ohkubo, Phys. Rev. Lett. **107**, 112501 (2011).
- [56] T. Suhara and Y. Kanada-En'yo, Phys. Rev. C **84**, 024328 (2011).
- [57] T. Mo and H. R. Weller, Phys. Rev. C **8**, 972 (1973).
- [58] Y. Kanada-En'yo, H. Morita and F. Kobayashi, arXiv:1504.02594 [nucl-th].
- [59] A. B. Volkov, Nucl. Phys. **74**, 33 (1965).
- [60] N. Yamaguchi, T. Kasahara, S. Nagata and Y. Akaishi, Prog. Theor. Phys. **62**, 1018 (1979); R. Tamagaki, Prog. Theor. Phys. **39**, 91 (1968).
- [61] F. Ajzenberg-Selove, Nucl. Phys. A **523**, 1 (1991).
- [62] A. Gallmann, F. Hibou, and P. Fintz, Nucl. Phys. A **123**, 27 (1969).
- [63] Y. Kanada-En'yo, T. Suhara and Y. Taniguchi, Prog. Theor. Exp. Phys. **2014**, 073D02 (2014).